Lensfree time-gated photoluminescent imaging

Maryam Baker[1] and Euan McLeod[1, a)]
Wyant College of Optical Sciences, University of Arizona, 1630 E. University Blvd., Tucson, AZ 85721, USA

(*Electronic mail: euanmc@optics.arizona.edu)

(Dated: 11 May 2023)

Fluorescence and, more generally, photoluminescence enable high contrast imaging of targeted regions of interest through the use of photoluminescent probes with high specificity for different targets. Fluorescence can be used for rare cell imaging, however this often requires a high space-bandwidth product: simultaneous high resolution and large field of view. With bulky traditional microscopes, high space-bandwidth product images require time-consuming mechanical scanning and stitching. Lensfree imaging can compactly and cost-effectively achieve a high space-bandwidth product in a single image through computational reconstruction of images from diffraction patterns recorded over the full field of view of standard image sensors. Many methods of lensfree photoluminescent imaging exist where the excitation light is filtered before the image sensor, often by placing spectral filters between the sample and sensor. However, the sample-to-sensor distance is one of the limiting factors on resolution in lensfree systems and so more competitive performance can be obtained if this distance is reduced. Here we show a time-gated lensfree photoluminescent imaging system that can achieve a resolution of 8.77 μm We use europium chelate fluorophores because of their long lifetime (642 μs) and trigger camera exposure approximately 50 μs after excitation. Because the excitation light is filtered temporally, there is no need for physical filters, enabling reduced sample-to-sensor distances and higher resolution.

I. INTRODUCTION

Lensfree on-chip imaging can achieve resolutions comparable to lens-based microscopes, but over larger fields of view and often in more cost-effective and smaller systems. Base components of a lensfree microscope comprise only a light source and an image sensor[1]. The imaging is done computationally, eliminating the need for expensive high NA aberration-corrected lenses or objectives[1]. Large field of view imaging without the need for mechanical scanning and image stitching is advantageous in pathology for imaging samples such as blood smears or histological tissue slices. Such microscopic imaging is the gold standard for diagnosing a number of diseases, including malaria and various forms of cancer. In many cases, the important features of interest are limited or sparsely distributed throughout the sample[2]. Fluorescent imaging can highlight many of these rare features through chemically labeling features of interest[3,4]. High-resolution fluorescent or photoluminescent lensfree imaging could enable better cytometry and virometry[5–10], biomolecular assays[11–14], or neural imaging[15–20]. However, achieving high resolution in photoluminescent lensfree imaging has remained a challenge because the incoherent nature of the emission precludes the use of holographic reconstruction or phase recovery techniques that have been used to reconstruct coherent lensfree images with wavelength-scale, or smaller, resolution[21–23].

For incoherent lensfree imaging, the smallest resolvable spot is approximately $2z_2$, corresponding to the full width at half maximum of the intensity radiated by a point source imaged across a perpendicular sensor plane at a distance of z_2. For high resolution, it is desirable to minimize the sample-to-sensor distance so that the diffracted spot is as small and bright as possible[5,24]. In standard fluorescence imaging, a spectral emission filter is placed somewhere between the sample and camera to exclude excitation light because the fluorescent emission is generally many orders of magnitude weaker than the excitation. In lensfree imaging, some method of excitation exclusion remains necessary, but the thickness of emission filters increases z_2, lowering resolution. Other complications of spectral filters in lensfree imaging include autofluorescence from the filter in the case of absorption filters, and angle-dependent transmission in the case of interference filters. Because light is emitted in all directions from the fluorophore and z_2 is small compared to the image sensor active area, much of the emitted light would impinge on the interference filter at a high incidence angle, where the spectral transimission is different from that for normally incident light.

Various hardware configurations can mitigate these challenges. As absorption filters are not angle dependent, they have been used in isolation in lensfree systems[5,16,25–29]. In these cases, high-performance custom filters are often used that have stronger absorption and smaller thicknesses than standard absorption filters, with minimal autofluorescence. More rarely, interference filters can be used in isolation[9,30], although the angle-dependent transmission property of such filters limits performance. Often, the two types of filters are combined so that the absorption filter blocks high-incidence angle excitation while the interference filter blocks any autofluorescence from the absorption filter together with any normal-incidence excitation that leaked through the absorption filter[17–20]. But the combination of multiple filters even further exacerbates the large z_2 distance, reducing resolution. Fiber-optic plates (faceplates) can be inserted into the optical train to allow for a larger z_2 without degrading resolution[6–8,15,31–34]. The array of waveguides in the fiber-optic plates guides the image without diffraction and, due to the limited numerical aperture of the fiber optics, also limits the transmission of high-incidence light. Particularly small z_2

a)http://wp.optics.arizona.edu/emcleod

values can be achieved by microfabricating spectral filtration structures directly on the image sensor, such as angle-sensitive gratings[17,30] or silo filters that guide light to each pixel[26]. Any of the above approaches can be combined with prisms or glass hemispheres before the sample to deliver the excitation such that total internal reflection of the background excitation reduces the amount of excitation light that reaches the image sensor[5,27,30,32,33].

Most of the fluorescent lensfree imaging techniques discussed above have resolution in the range of 10–50 μm[5,7–9,15–18,26,27,32,34], while a few have significantly poorer resolution at 500 μm[25,30], and several have resolution in the range of 1.2–9 μm[19,20,28,29,33,35]. All of these examples of resolution better than 10 μm rely on computational techniques to improve the resolution significantly beyond the hardware-alone limit of $\sim 2z_2$. These techniques include compressive sampling to localize sparse source points[33,35], scanning of an excitation Talbot spot array[29], as well as micro or nano-structured phase and/or amplitude masks that introduce a shift-variant point spread function that can be later decoded assuming a prior calibration step[19,20,28,35]. Some compact lens-based fluorescence imaging devices have utilized shift-invariant point spread functions (PSFs) using a microlens array to achieve resolutions as low as 7 μm[36].

Here, we present a novel hardware approach for rejecting the excitation light in lensfree imaging that relies on time-gated photoluminescence (Figure 1), which has been used in conventional lens-based microscopy[37]. Time gating removes the need for any optical components between the sample and sensor, enabling smaller z_2 distances, which can lead to improved resolution. Here we demonstrate 8.77 μm resolution without any complex computational approaches to improve resolution. By combining our approach with computational techniques like those above, we could achieve better resolution in future work. Time-gated photoluminescence imaging is a means for overcoming tissue auto-fluorescence[34] as well as increasing image contrast[38] by eliminating any scattered light from the excitation source. Many long-lifetime probes have been developed for time-gated imaging with photoluminescent lifetimes on the order of microseconds[39–42].

Other important time-gated photoluminescent imaging modalities include fluorescence lifetime imaging microscopy (FLIM)[43,44] and time-gated fluorescence correlation spectroscopy (FCS)[45], which utilize fluorescence lifetimes to distinguish different probes. Like lensfree imaging, wide-field illumination has been used for large FOV imaging in FLIM[46] and FCS[47]. To achieve wide-field images for FLIM, light sheet illumination has been used to excite probes over the whole extent of the sample such as such as *C. elegans* or cancer cell spheroids[46]. For FCS, single plane illumination fluorescence microscopy (SPIM) has been combined with FCS, utilizing light sheet illumination in a single plane to image samples in different z-planes[47]. Cameras such as EMCCDs and CMOS sensors have also been used for imaging FCS[47–49]. However, for the low-light and fast-time scale experiments done using FCS, such as diffusion coefficient and concentration measurements, camera characteristics have to be considered such as noise and frame rate to ensure the accuracy of measurements[48,49].

The combination of application specific long-lifetime probes and the elimination of sample auto-fluorescence enabled time-gated photoluminescence to provide further insight into cell dynamics, such as single tumor cells in the bloodstream[50,51] and live cancer cells[52].Time-gated photoluminescence imaging also has other applications, such as for use in tomography[53]. We demonstrate lensfree time-gated imaging of europium chelate nanoparticles with a luminescence lifetime of ∼600 μs deposited on a resolution target. However, this system can be adapted for use with other long-lifetime luminescent probes such as lanthanide chelates and lanthanide-doped nanocrystals with lifetimes ranging from μs to ms[39] or porous silicon nanoparticles with a lifetime of 5-13 μs[34]. Lanthanide doped nanoparticles can be used for probing human cervical carcinoma (HeLa) cells[39] or cellular mitochondria[54] and porous silicon nanoparticles can be used for screening ovarian cancer[34].

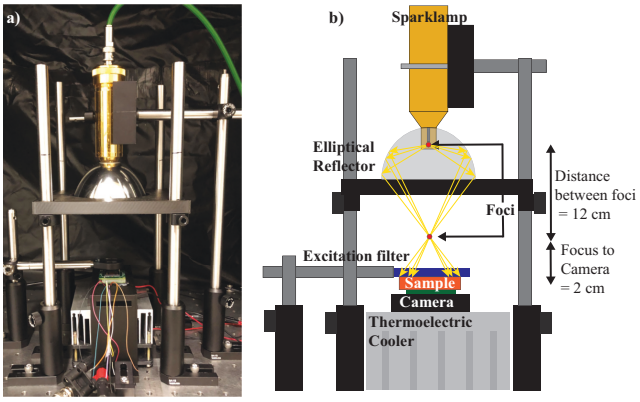

FIG. 1. Experimental lensfree time-gated photoluminescence setup. (a) Photograph. (b) Diagram.

Currently, the closest application of time-gated photoluminescence to lensfree imaging uses single photon avalanche diode (SPAD) arrays for applications such as neural imaging[55], or fluorescence lifetime imaging[56]. But these arrays are typically quite small in number with large pitch, e.g., an 8×64 array with 25 μm pitch, resulting in relatively low resolution, e.g. $63 \times 26 \times 51$ μm voxel size for the smallest resolvable spot[55]. Lens-based SPAD imaging exists and improves collection efficiency of each pixel with a microlens[57], a variable important for high-speed[58] low-light imaging. There are also lens-based SPAD imaging systems that combine FLIM and FCS[59,60]. However these systems lack the compact form-factor of lensfree SPAD imaging desirable for *in-vivo* imaging. Here we show a time-gated lensfree photoluminescence imaging system using a CMOS sensor that has the benefits of a much larger pixel count (3.2 MP), with small pixel size (3.45 μm) over a large field-of-view (7.06 x 5.3 mm). This field-of-view is comparable to most other lensfree microscopes, which are based on mass-produced CMOS sensors.

II. METHODS

A. Photoluminescent Nanoparticles

The photoluminescent probes used were 300 nm diameter spherical particles (Fluoromax ThermoFisher 2947-0701-011150, Bangs Lab FCEU003) doped with europium chelate (EC), $\lambda_{\text{excitation}}$ = 330–340 nm and $\lambda_{\text{emission}}$ = 610–620 nm, which are fluorophores with long lifetimes on the order of 0.5 ms[61]. The long photoluminescence lifetime compared to the typical few nanosecond lifetime of most fluorophores relaxes the timing tolerances for time-gating and improves the image signal-to-noise ratio (SNR) as there is a large window over which to collect emitted photons. Due to the lifetime of the fluorophore being on the order of hundreds of µs, we use the term photoluminescence.

B. Excitation source

Figure 1 shows the components used for the lensfree imaging portion of the experiment. An elliptical reflector (Edmund # 68-797) was used to maximize collection efficiency of the spark lamp (Nanolite KL-M) emission that is directed onto the sample and used to excite the EC, beyond the more limited collection efficiency offered by a lens. A bandpass excitation filter (Edmund # 86-981), $\Delta\lambda$ = 333-381 nm, was placed between the spark lamp and the sample to reduce the background from blackbody emission from the electrodes of the spark lamp that result from heat generated by the spark. This blackbody emission occurs over a relatively long timescale and cannot be rejected by microsecond-scale time gating, as shown in Section III A.

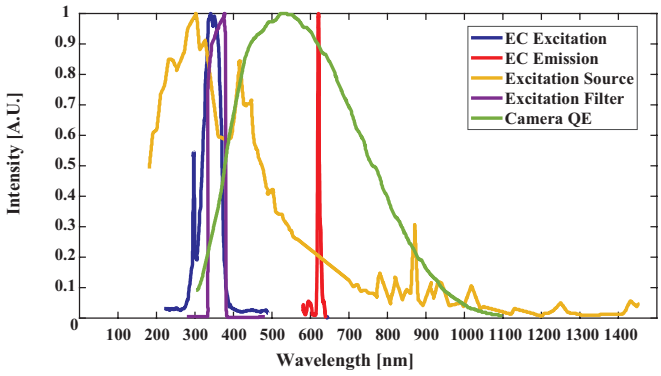

FIG. 2. Spectral curves for europium chelate (EC) imaging. All curves are normalized to a peak value of 1. EC excitation and emission data are from reference[62]. Spark lamp excitation source data are from reference[63]. Filter data are from reference[64]. Image sensor quantum efficiency (QE) data are from reference[65].

C. Camera

A monochrome machine vision camera (FLIR CM3-U3-314SM-CS) was used to image the emission from the nanoparticles. The coverglass was removed from the camera by the company Pacific X-ray in order to minimize z_2. A thermoelectric cooler (Adafruit 1335) was placed under the camera to keep it between 29°C–46°C in order to reduce thermal noise. A design goal of this work was to keep the system as low-cost and comprised of as many off-the-shelf parts as possible and so although bulky, the thermoelectric cooler was used for its low cost, availability, and sufficient performance.

D. Spectral Considerations

Figure 2 shows the relevant spectra for EC imaging. EC is most efficiently excited in the near UV, around 350 nm, while its emission is predominantly narrowband at 610 nm. Our spark lamp excitation source peaks in the near UV, matching well with the EC excitation spectrum. The excitation bandpass filter is used to reject visible and IR light from the source, which would have provided little EC excitation and also contributed to a long tail of background emission from the spark lamp due to blackbody radiation, as discussed in Section II B. The quantum efficiency curve of the image sensor overlaps well with the EC emission, while showing reduced sensitivity to the UV excitation, further aiding image contrast.

E. Time-Gating

The emission from the luminescing nanoparticles was filtered in time from the spark lamp excitation by delaying the start of the camera exposure from the start of the spark lamp, as shown in Figure 3. An image capture sequence was initiated by a pulse from an NI-DAQ (782602-01) to a pulse delay generator (DG535) to initiate two subsequent pulses: one pulse to trigger the spark lamp (output A) and another pulse to trigger the camera exposure (output B). To exclude the excitation light from the captured frame via time-gating, the necessary delay between output B and output A depended on the pulse width of the light emitted from the spark lamp as well as electronic delays inherent to the spark lamp controller and the camera interface board. The spark lamp had a quoted pulse width of 11 ns, but blackbody emission from the electrodes of the spark lamp exhibited a much longer tail (tens–hundreds of microseconds) due to heating resulting from the spark. Although weak compared to the primary pulse, this emission tail was long enough to introduce unwanted background signal into our images unless filtered correctly. As described above, we used a UV bandpass filter to effectively shorten the tail of the spark lamp emission without significantly reducing the excitation efficiency of the photoluminescent particles.

Another aspect of time-gating systems necessary to consider is that the intensity of the excitation source is often at least an order of magnitude higher than the photoluminescent

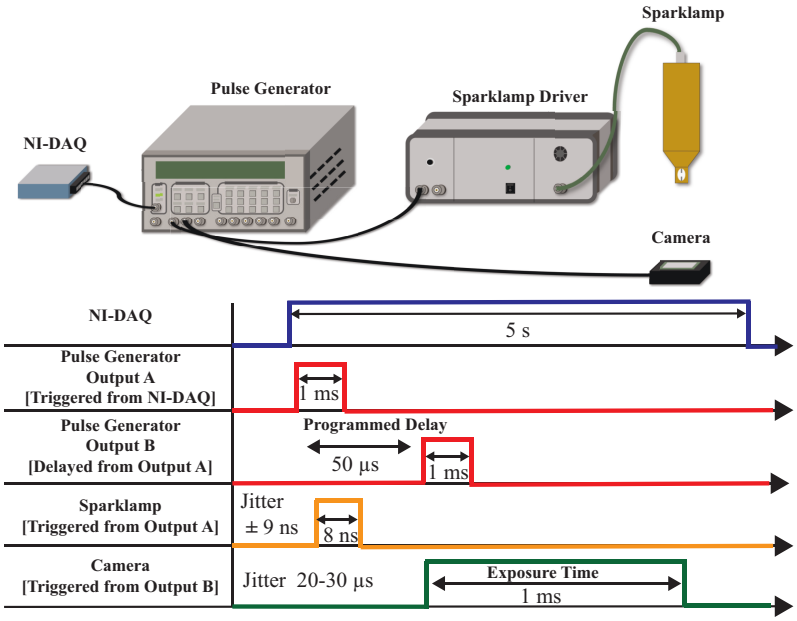

FIG. 3. Timing diagram for time-gated imaging (not to scale). The jitter noted in front of the spark lamp and camera curves describes the range of timing delays due to the electrical response of each device's internal circuitry.

emission from the sample. Any light from the spark lamp incident on the camera would saturate the sensor, leaving any recorded photoluminescence emission indistinguishable. To mitigate this, the delay between the trigger pulse and start of the exposure had to be measured as well as the jitter on the start of the exposure. For the camera used, a jitter of 20-30 µs was measured.

III. RESULTS & DISCUSSION

A. Timing optimization

The magnitude of the unwanted IR emission can be inferred from the difference between the two curves in Figure 4a, corresponding to the apparent decay of the spark lamp with and without the UV bandpass filter between the source and the camera. The exposure time for these experiments was 5 ms, which is effectively infinity with respect to the time scale of the spark lamp pulse (manufacturer's specification of 11 ns) and europium chelate lifetime (∼500 µs). For each curve, the beginnings and tails of the curves are separately fit to exponential decays:

$$y = Ae^{-t/\tau} \tag{1}$$

The domains of these fits and resulting time constants τ are shown in Table I. Note that the experimental data measures the integrated light energy over the exposure, and not the instantaneous light intensity. However, both quantities share the same time constant, assuming an exponential decay. At short times, the recorded emission from the spark lamp decays faster with the bandpass filter ($\tau = 1.38$ µs) than without the filter ($\tau = 3.98$ µs), as the thermal emission is filtered out, enabling a shorter delay time between the spark lamp pulse and the start of the camera exposure, resulting in a greater number of collected photoluminescence emission photons. With the filter in place, the observed excitation rapidly reaches the noise floor of the image sensor, as desired.

The time at which the emission from the spark lamp becomes negligible was determined using Figure 4b, which compares the emission from the bandpass-filtered spark lamp with the emission from the EC. These values are plotted in terms of SNR:

$$\mathrm{SNR} = \frac{\mu_s - \mu_b}{\sigma_b}, \tag{2}$$

where μ_s is the mean signal value, μ_b is the mean background value, and σ_b is the standard deviation of a background image. For the excitation curve, the signal image was acquired without any sample between the light source and the image sensor. The background images are acquired where the spark lamp is disconnected. These are important for removing noise inherent to the sensor, i.e. dark current. Background and signal images were time-matched from the start of the experiment because the time-gated system becomes more thermally stable and less noisy over time. To better measure the decay of the source at long time scales, the measurements in Figure 4b were acquired with a high-dynamic range camera (PI-MAX 4 Teledyne Princeton Instruments), whereas all the other measurements presented in this paper were taken with the machine vision camera described in Section II C.

The spark lamp SNR is at least an order of magnitude smaller than the EC SNR for $t > 50$ µs, and so a 50 µs delay was programmed into the system and used for all following images. However, due to camera jitter, the true delay could

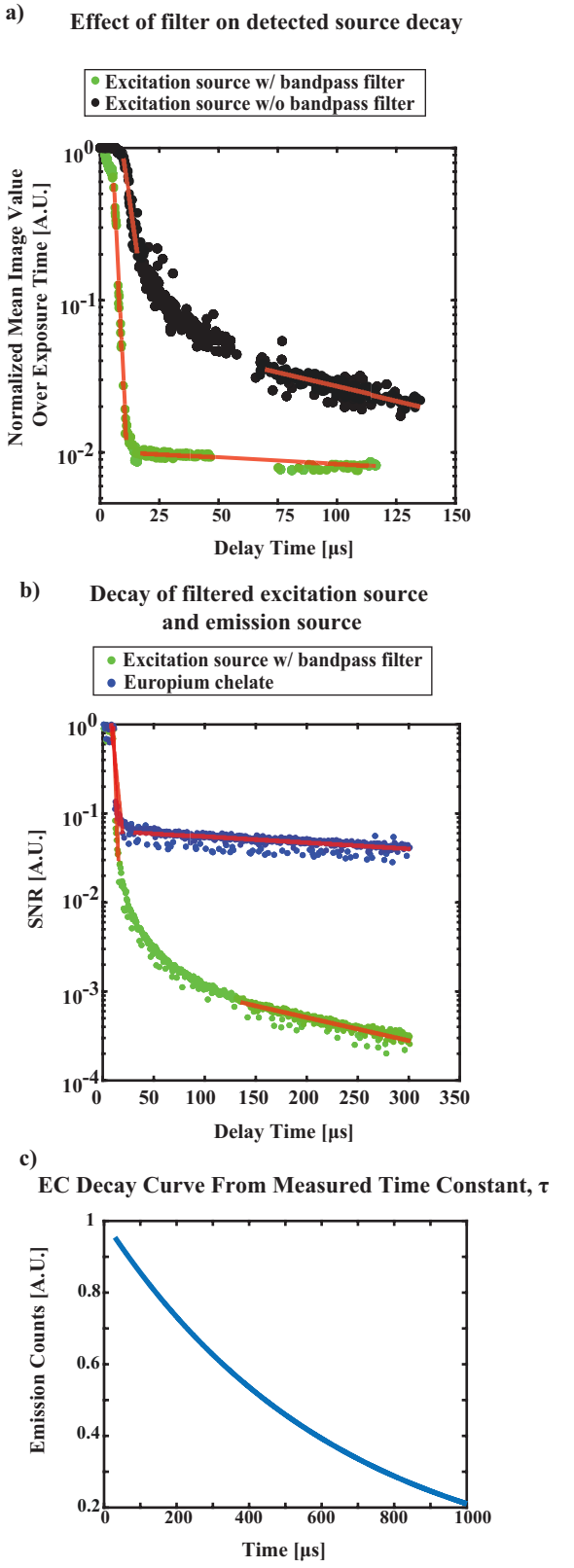

FIG. 4. Excitation and emission lifetimes. (a) Light energy collected by the image sensor as a function of the delay between the spark lamp pulse and the start of exposure, with and without a UV bandpass filter placed between the light source and the sample. (b) SNR of light collected by the image sensor as a function of the delay between the spark lamp pulse and the start of exposure. The UV bandpass filter was in place for both curves, but only the europium chelate curve was acquired using a sample with photoluminescent particles. (c) Lifetime of EC from measured time constant $\tau = 642$ in Table I using equation (1).

TABLE I. Decay time constants resulting from exponential fits.

Fig. 4 panel	Source	UV bandpass filter in place	Time Range [μs]	τ [μs]
a	Spark lamp	✓	5.85–11.18	1.38
a	Spark lamp	✓	17.30–116.35	500.
a	Spark lamp	×	10.15–15.81	3.98
a	Spark lamp	×	69.65–135.19	120.
b	Spark lamp	✓	10.50–15.50	1.45
b	Spark lamp	✓	136.00–301.00	168
b	Europium chelate	✓	8.00–19.50	3.82
b	Europium chelate	✓	30.50–301.00	642

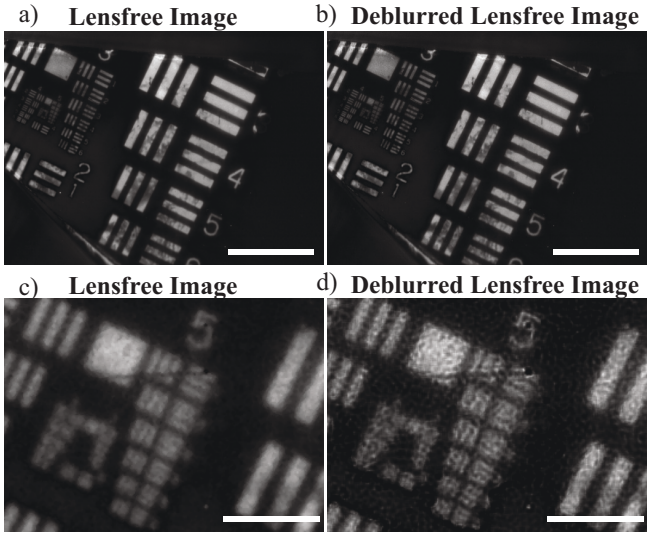

FIG. 5. Resolution characterization. a) Image without any deblurring algorithm. b) Panel a) with a Lucy-Richardson deblurring filter applied in MATLAB. c) Panel a) zoomed in to show Group 5. d) Panel b) zoomed in to show improved resolution of Group 5. The scale bars in a) and b) are 2 mm and the scale bars in c) and d) are 250 μm.

vary by a few tens of microseconds. An output pulse from the camera was monitored to determine the true delay for each image. The lifetime of the EC emission was found from the exponential fit at long decay times to be 642 μs, which is consistent with the estimated lifetime of 500 μs quoted in the data sheet[62]. The apparent short lifetime at delay times less than 20 μs is an artifact of the spark lamp excitation that remains strong at these short delay times.

B. Resolution

The image resolution was characterized using an opaque-background USAF 1951 resolution target (Edmund Optics). The target was made photoluminescent by coating one side with a dense layer of EC particles. This side was then placed facing the image sensor. 1000 raw frames with delays of 60–80 μs were averaged to produce the images in Figure 5. Fig-

ure 5c shows a close up of Group 5. The contrast of the pattern can be improved via simple deblurring (Figure 5b and d) performed in MATLAB using the Lucy-Richardson deconvolution method over 10 iterations assuming a Gaussian point spread function with a size 5×5 pixels and $\sigma = 5$, where σ is the standard deviation of the Gaussian filter. The full width at half the maximum of the Gaussian PSF is 12 pixels. The filter parameters, size and σ, were varied and selected based on the smallest visually resolvable element of the resolution target. From these images, the smallest resolvable element is now Group 5 Element 6 with a line width of 8.77 μm.

C. Image Averaging

For each experiment, 1000 frames were taken and averaged. Figure 6 shows the impact on the SNR of the average image as more frames are included Figure 6a shows a fit of the SNR data to a square-root dependence. A square root function was fitted, assuming that the signal is uncorrelated to the noise and that the noise is random with zero mean and constant variance, causing the averaged noise to become reduced by the square of the number of images. We attribute deviations between the experimental data and the fit to thermally-varying noise levels as the sensor heats up over the first few images and eventually stabilizes.

D. Sensitivity & Dynamic Range

To demonstrate the dynamic range of the system, samples of decreasing photoluminescent particle concentrations were imaged in the time-gated system. Figure 7 shows that sample concentrations spanning two orders of magnitude can be imaged, indicating applicability to more typical low fluorescent labeling densities.

IV. CONCLUSION

Here we show a time-gated lensfree photoluminescence imaging system that is able to achieve a resolution of 8.77 μm over a large field of view (7.06 x 5.3 mm) where the resolution is maintained across the whole FOV except for a thin border at the edge of the sensor of width $\sim z_2$, or approximately 4 μm. By eliminating all elements between the sample and the sensor and temporally filtering out the excitation light, we are able to improve the SNR of the image and consequently the resolution. The system is currently limited to planar samples. In future work, the resolution could be improved by implementation of more computational techniques such as compressive sensing, which utilizes measurement of the system PSF to estimate an image from the blurry image with an l_1-regularized least squares optimization approach[33].

Although in its current configuration, this lensfree system relies on some relatively expensive and bulky components, it is still cheaper and less bulky than most commercially available lens-based fluorescence imaging systems and is easily adaptable to a range of photoluminescent probes. In the future, more cost-effective and compact light sources and timing electronics could be used. The footprint of the timing electronics could be reduced using a compact pulse delay generator such as an AeroDIODE TOMBAK. The TOMBAK is palm-sized, 104 x 95x 28.2 mm, and is capable of pulse delays as short as 10 ps. The illumination source and elliptical reflector could be replaced with a smaller illumination source, such as a NanoLED. Although the NanoLED would restrict the system to operating at a single wavelength, NanoLEDs could be swapped depending on the necessary excitation wavelength.

ACKNOWLEDGEMENTS

We would like to acknowledge Kenneth Lang for helpful discussions. This work was supported by the National Science Foundation under award number ECCS-2114275.

AUTHOR DECLARATIONS

Conflict of Interest

Drs. Baker and McLeod are inventors on intellectual property related to lensfree imaging.

Author Contributions

Maryam Baker: Methodology (lead); Investigation (lead); Writing/Original Draft Preparation (lead); Writing/Review & Editing (equal) Euan McLeod: Conceptualization (lead); Funding Acquisition (lead); Methodology (supporting); Supervision (lead); Writing/Review & Editing (equal)

DATA AVAILABILITY

Data underlying the results presented in this paper are not publicly available at this time but may be obtained from the authors upon reasonable request.

[1] A. Ozcan and E. McLeod, "Lensless Imaging and Sensing," Annual Review of Biomedical Engineering **18**, 77–102 (2016), _eprint: https://doi.org/10.1146/annurev-bioeng-092515-010849.

[2] Y. Zhang, A. Greenbaum, W. Luo, and A. Ozcan, en"Wide-field pathology imaging using on-chip microscopy," Virchows Archiv **467**, 3–7 (2015).

[3] M. Renz, en"Fluorescence microscopy—A historical and technical perspective," Cytometry Part A **83**, 767–779 (2013), _eprint: https://onlinelibrary.wiley.com/doi/pdf/10.1002/cyto.a.22295.

[4] R. Heim and R. Y. Tsien, eng"Engineering green fluorescent protein for improved brightness, longer wavelengths and fluorescence resonance energy transfer," Current biology: CB **6**, 178–182 (1996).

[5] A. F. Coskun, T.-W. Su, and A. Ozcan, en"Wide field-of-view lens-free fluorescent imaging on a chip," Lab on a Chip **10**, 824–827 (2010), publisher: The Royal Society of Chemistry.

[6] S. A. Arpali, C. Arpali, A. F. Coskun, H.-H. Chiang, and A. Ozcan, en"High-throughput screening of large volumes of whole blood using structured illumination and fluorescent on-chip imaging," Lab on a Chip **12**, 4968–4971 (2012), publisher: The Royal Society of Chemistry.

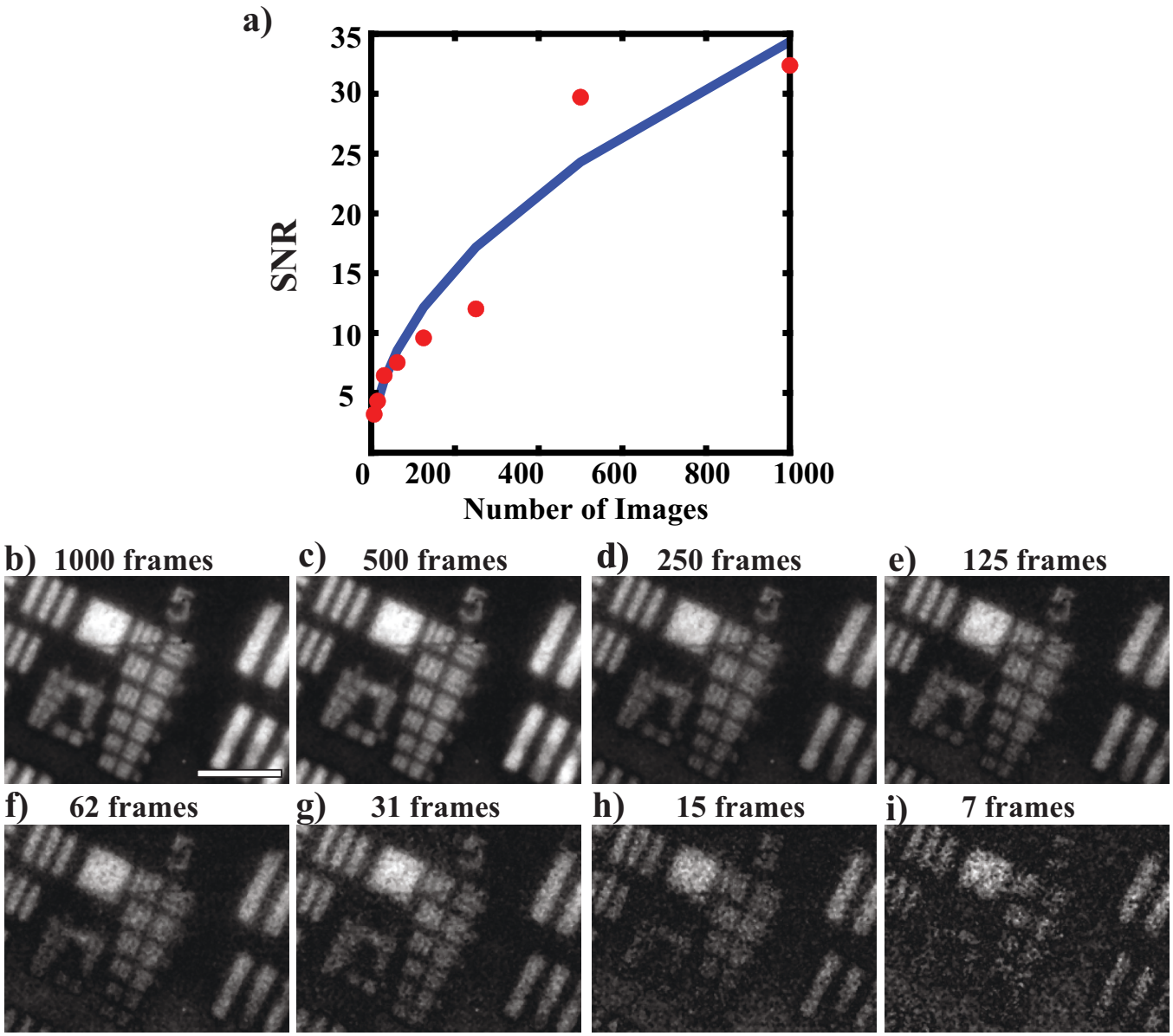

FIG. 6. Improved SNR through frame averaging. (a) SNR based on averaging different subsets of acquired frames. The blue line shows a square root fit, $y = 1.0864\sqrt{x}$. (b–i) Images of the resolution target based on averaging different numbers of frames. The scale bar is 250 μm.

[7] K. Sasagawa, A. Kimura, M. Haruta, T. Noda, T. Tokuda, and J. Ohta, EN"Highly sensitive lens-free fluorescence imaging device enabled by a complementary combination of interference and absorption filters," Biomedical Optics Express **9**, 4329–4344 (2018), publisher: Optica Publishing Group.

[8] H. Takehara, O. Kazutaka, M. Haruta, T. Noda, K. Sasagawa, T. Tokuda, and J. Ohta, "On-chip cell analysis platform: Implementation of contact fluorescence microscopy in microfluidic chips," AIP Advances **7**, 095213 (2017), publisher: American Institute of Physics.

[9] K. Imai, M. Nishigaki, Y. Onozuka, Y. Akimoto, M. Nagai, S. Matsumoto, and S. Kousai, "A lens-free single-shot fluorescent imaging system using CMOS image sensors with dielectric multi-layer filter," in *2017 19th International Conference on Solid-State Sensors, Actuators and Microsystems (TRANSDUCERS)* (2017) pp. 139–142, iSSN: 2167-0021.

[10] A. Ray, M. U. Daloglu, J. Ho, A. Torres, E. Mcleod, and A. Ozcan, en"Computational sensing of herpes simplex virus using a cost-effective on-chip microscope," Scientific Reports **7**, 4856 (2017), number: 1 Publisher: Nature Publishing Group.

[11] K. Sasagawa, S. H. Kim, K. Miyazawa, H. Takehara, T. Noda, T. Tokuda, R. Iino, H. Noji, and J. Ohta, "Dual-mode lensless imaging device for digital enzyme linked immunosorbent assay," in *Frontiers in Biological Detection: From Nanosensors to Systems VI*, Vol. 8933 (SPIE, 2014) pp. 106–111.

[12] M. U. Daloglu, A. Ray, Z. Gorocs, M. Xiong, R. Malik, G. Bitan, E. McLeod, and A. Ozcan, en"Computational On-Chip Imaging of Nanoparticles and Biomolecules using Ultraviolet Light," Scientific Reports **7**, 44157 (2017), number: 1 Publisher: Nature Publishing Group.

[13] Z. Xiong, C. J. Potter, and E. McLeod, "High-Speed Lens-Free Holographic Sensing of Protein Molecules Using Quantitative Agglutination Assays," ACS Sensors **6**, 1208–1217 (2021), publisher: American Chemical Society.

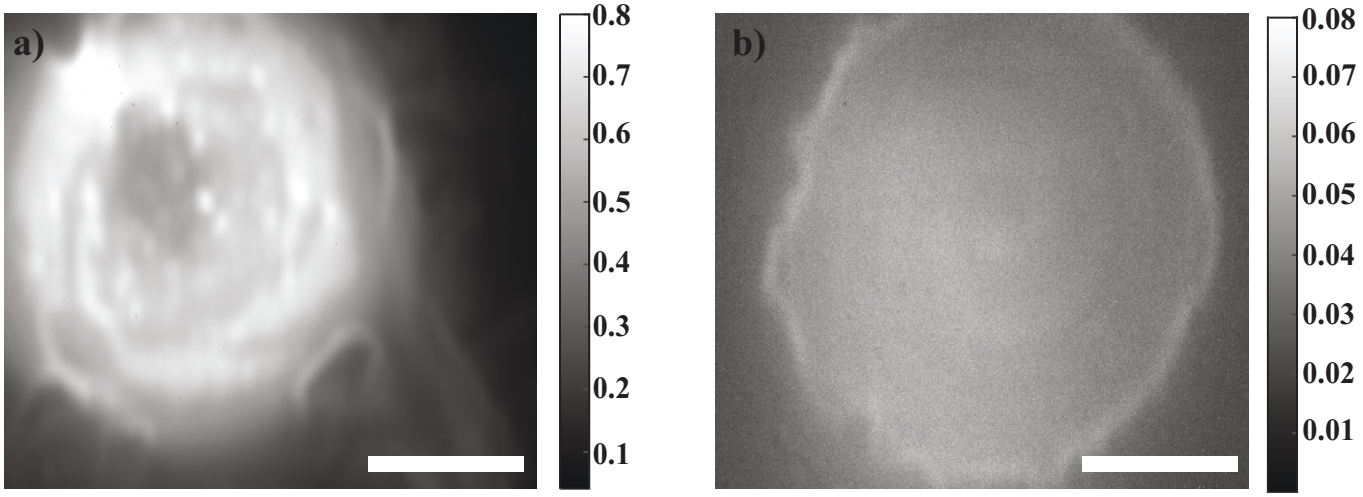

FIG. 7. Ability to detect a range of concentrations of nanoparticles. a) ∼667 million 300 nm EC particles. b) ∼2 million 300 nm EC particles. The scale bars are 2.1 mm.

[14] C. J. Potter, Y. Hu, Z. Xiong, J. Wang, and E. McLeod, en"Point-of-care SARS-CoV-2 sensing using lens-free imaging and a deep learning-assisted quantitative agglutination assay," Lab on a Chip **22**, 3744–3754 (2022), publisher: The Royal Society of Chemistry.

[15] K. Sasagawa, Y. Ohta, M. Kawahara, M. Haruta, T. Tokuda, and J. Ohta, "Wide field-of-view lensless fluorescence imaging device with hybrid band-pass emission filter," AIP Advances **9**, 035108 (2019), publisher: American Institute of Physics.

[16] A. K. Mudraboyina, L. Blockstein, C. C. Luk, N. I. Syed, and O. Yadid-Pecht, "A Novel Lensless Miniature Contact Imaging System for Monitoring Calcium Changes in Live Neurons," IEEE Photonics Journal **6**, 1–15 (2014), conference Name: IEEE Photonics Journal.

[17] A. J. Taal, C. Lee, J. Choi, B. Hellenkamp, and K. L. Shepard, en"Toward implantable devices for angle-sensitive, lens-less, multifluorescent, single-photon lifetime imaging in the brain using Fabry–Perot and absorptive color filters," Light: Science & Applications **11**, 24 (2022), number: 1 Publisher: Nature Publishing Group.

[18] E. Rustami, K. Sasagawa, K. Sugie, Y. Ohta, M. Haruta, T. Noda, T. Tokuda, and J. Ohta, "Needle-Type Imager Sensor With Band-Pass Composite Emission Filter and Parallel Fiber-Coupled Laser Excitation," IEEE Transactions on Circuits and Systems I: Regular Papers **67**, 1082–1091 (2020), conference Name: IEEE Transactions on Circuits and Systems I: Regular Papers.

[19] G. Kuo, F. L. Liu, I. Grossrubatscher, R. Ng, and L. Waller, EN"On-chip fluorescence microscopy with a random microlens diffuser," Optics Express **28**, 8384–8399 (2020), publisher: Optica Publishing Group.

[20] J. K. Adams, D. Yan, J. Wu, V. Boominathan, S. Gao, A. V. Rodriguez, S. Kim, J. Carns, R. Richards-Kortum, C. Kemere, A. Veeraraghavan, and J. T. Robinson, en"In vivo lensless microscopy via a phase mask generating diffraction patterns with high-contrast contours," Nature Biomedical Engineering **6**, 617–628 (2022), number: 5 Publisher: Nature Publishing Group.

[21] E. McLeod, W. Luo, O. Mudanyali, A. Greenbaum, and A. Ozcan, en"Toward giga-pixel nanoscopy on a chip: a computational wide-field look at the nano-scale without the use of lenses," Lab on a Chip **13**, 2028–2035 (2013), publisher: The Royal Society of Chemistry.

[22] E. McLeod and A. Ozcan, en"Unconventional methods of imaging: computational microscopy and compact implementations," Reports on Progress in Physics **79**, 076001 (2016), publisher: IOP Publishing.

[23] W. Luo, A. Greenbaum, Y. Zhang, and A. Ozcan, en"Synthetic aperture-based on-chip microscopy," Light: Science & Applications **4**, e261–e261 (2015), number: 3 Publisher: Nature Publishing Group.

[24] A. Shanmugam and C. D. Salthouse, "Lensless fluorescence imaging with height calculation," Journal of Biomedical Optics **19**, 016002 (2014), publisher: SPIE.

[25] E. P. Papageorgiou, H. Zhang, B. E. Boser, C. Park, and M. Anwar, EN"Angle-insensitive amorphous silicon optical filter for fluorescence contact imaging," Optics Letters **43**, 354–357 (2018), publisher: Optica Publishing Group.

[26] S. A. Lee, X. Ou, J. E. Lee, and C. Yang, EN"Chip-scale fluorescence microscope based on a silo-filter complementary metal-oxide semiconductor image sensor," Optics Letters **38**, 1817–1819 (2013), publisher: Optica Publishing Group.

[27] A. F. Coskun, I. Sencan, T.-W. Su, and A. Ozcan, en"Lensfree Fluorescent On-Chip Imaging of Transgenic Caenorhabditis elegans Over an Ultra-Wide Field-of-View," PLOS ONE **6**, e15955 (2011), publisher: Public Library of Science.

[28] J. K. Adams, V. Boominathan, B. W. Avants, D. G. Vercosa, F. Ye, R. G. Baraniuk, J. T. Robinson, and A. Veeraraghavan, "Single-frame 3D fluorescence microscopy with ultraminiature lensless FlatScope," Science Advances **3**, e1701548 (2017), publisher: American Association for the Advancement of Science.

[29] C. Han, S. Pang, D. V. Bower, P. Yiu, and C. Yang, "Wide Field-of-View On-Chip Talbot Fluorescence Microscopy for Longitudinal Cell Culture Monitoring from within the Incubator," Analytical Chemistry **85**, 2356–2360 (2013), publisher: American Chemical Society.

[30] E. P. Papageorgiou, H. Zhang, S. Giverts, C. Park, B. E. Boser, and M. Anwar, EN"Real-time cancer detection with an integrated lensless fluorescence contact imager," Biomedical Optics Express **9**, 3607–3623 (2018), publisher: Optica Publishing Group.

[31] E. Yıldırım, Arpali, and S. A. Arpali, en"Implementation and characterization of an absorption filter for on-chip fluorescent imaging," Sensors and Actuators B: Chemical **242**, 318–323 (2017).

[32] A. F. Coskun, I. Sencan, T.-W. Su, and A. Ozcan, EN"Lensless wide-field fluorescent imaging on a chip using compressive decoding of sparse objects," Optics Express **18**, 10510–10523 (2010), publisher: Optica Publishing Group.

[33] A. F. Coskun, I. Sencan, T.-W. Su, and A. Ozcan, en"Wide-field lensless fluorescent microscopy using a tapered fiber-optic faceplate on a chip," Analyst **136**, 3512–3518 (2011), publisher: The Royal Society of Chemistry.

[34] L. Gu, D. J. Hall, Z. Qin, E. Anglin, J. Joo, D. J. Mooney, S. B. Howell, and M. J. Sailor, en"In vivo time-gated fluorescence imaging with biodegradable luminescent porous silicon nanoparticles," Nature Communications **4**, 2326 (2013), number: 1 Publisher: Nature Publishing Group.

[35] B. Khademhosseinieh, I. Sencan, G. Biener, T.-W. Su, A. F. Coskun, D. Tseng, and A. Ozcan, "Lensfree on-chip imaging using nanostructured surfaces," Applied Physics Letters **96**, 171106 (2010), publisher: American Institute of Physics.

[36] Y. Xue, I. G. Davison, D. A. Boas, and L. Tian, "Single-shot 3D wide-field fluorescence imaging with a Computational Miniature Mesoscope,"

Science Advances **6**, eabb7508 (2020), publisher: American Association for the Advancement of Science.

[37] W. Yang and S.-L. Chen, "Time-gated fluorescence imaging: Advances in technology and biological applications," Journal of Innovative Optical Health Sciences **13**, 2030006 (2020), publisher: World Scientific Publishing Co.

[38] G. Nishimura, EN"Contrast improvement in indocyanine green fluorescence sensing in thick tissue using a time-gating method," Biomedical Optics Express **10**, 1234–1249 (2019), publisher: Optica Publishing Group.

[39] K. Y. Zhang, Q. Yu, H. Wei, S. Liu, Q. Zhao, and W. Huang, "Long-Lived Emissive Probes for Time-Resolved Photoluminescence Bioimaging and Biosensing," Chemical Reviews **118**, 1770–1839 (2018), publisher: American Chemical Society.

[40] F. Ni, N. Li, L. Zhan, and C. Yang, en"Organic Thermally Activated Delayed Fluorescence Materials for Time-Resolved Luminescence Imaging and Sensing," Advanced Optical Materials **8**, 1902187 (2020), _eprint: https://onlinelibrary.wiley.com/doi/pdf/10.1002/adom.201902187.

[41] B. del Rosal, D. H. Ortgies, N. Fernández, F. Sanz-Rodríguez, D. Jaque, and E. M. Rodríguez, "Overcoming Autofluorescence: Long-Lifetime Infrared Nanoparticles for Time-Gated In Vivo Imaging," Advanced Materials **28**, 10188–10193 (2016), _eprint: https://onlinelibrary.wiley.com/doi/pdf/10.1002/adma.201603583.

[42] M. Tan, B. d. Rosal, Y. Zhang, E. M. Rodríguez, J. Hu, Z. Zhou, R. Fan, D. H. Ortgies, N. Fernández, I. Chaves-Coira, Núñez, D. Jaque, and G. Chen, en"Rare-earth-doped fluoride nanoparticles with engineered long luminescence lifetime for time-gated in vivo optical imaging in the second biological window," Nanoscale **10**, 17771–17780 (2018), publisher: The Royal Society of Chemistry.

[43] R. Datta, T. M. Heaster, J. T. Sharick, A. A. Gillette, and M. C. Skala, "Fluorescence lifetime imaging microscopy: fundamentals and advances in instrumentation, analysis, and applications," Journal of Biomedical Optics **25**, 071203 (2020).

[44] E. P. Buurman, R. Sanders, A. Draaijer, H. C. Gerritsen, J. J. F. van Veen, P. M. Houpt, and Y. K. Levine, en"Fluorescence lifetime imaging using a confocal laser scanning microscope," Scanning **14**, 155–159 (1992), _eprint: https://onlinelibrary.wiley.com/doi/pdf/10.1002/sca.4950140305.

[45] D. C. Lamb, A. Schenk, C. Röcker, C. Scalfi-Happ, and G. U. Nienhaus, "Sensitivity enhancement in fluorescence correlation spectroscopy of multiple species using time-gated detection." Biophysical Journal **79**, 1129–1138 (2000).

[46] L. M. Hirvonen, J. Nedbal, N. Almutairi, T. A. Phillips, W. Becker, T. Conneely, J. Milnes, S. Cox, S. Stürzenbaum, and K. Suhling, en"Lightsheet fluorescence lifetime imaging microscopy with wide-field time-correlated single photon counting," Journal of Biophotonics **13**, e201960099 (2020), _eprint: https://onlinelibrary.wiley.com/doi/pdf/10.1002/jbio.201960099.

[47] T. Wohland, X. Shi, J. Sankaran, and E. H. K. Stelzer, EN"Single Plane Illumination Fluorescence Correlation Spectroscopy (SPIM-FCS) probes inhomogeneous three-dimensional environments," Optics Express **18**, 10627–10641 (2010), publisher: Optica Publishing Group.

[48] J. Sankaran, N. Bag, R. S. Kraut, and T. Wohland, "Accuracy and Precision in Camera-Based Fluorescence Correlation Spectroscopy Measurements," Analytical Chemistry **85**, 3948–3954 (2013), publisher: American Chemical Society.

[49] N. Bag, J. Sankaran, A. Paul, R. S. Kraut, and T. Wohland, en"Calibration and Limits of Camera-Based Fluorescence Correlation Spectroscopy: A Supported Lipid Bilayer Study," ChemPhysChem **13**, 2784–2794 (2012), _eprint: https://onlinelibrary.wiley.com/doi/pdf/10.1002/cphc.201200032.

[50] T. Pons, S. Bouccara, V. Loriette, N. Lequeux, S. Pezet, and A. Fragola, "In Vivo Imaging of Single Tumor Cells in Fast-Flowing Bloodstream Using Near-Infrared Quantum Dots and Time-Gated Imaging," ACS Nano **13**, 3125–3131 (2019), publisher: American Chemical Society.

[51] Y. Y. Hui, L.-J. Su, O. Y. Chen, Y.-T. Chen, T.-M. Liu, and H.-C. Chang, en"Wide-field imaging and flow cytometric analysis of cancer cells in blood by fluorescent nanodiamond labeling and time gating," Scientific Reports **4**, 5574 (2014), number: 1 Publisher: Nature Publishing Group.

[52] C.-C. Tu, K. Awasthi, K.-P. Chen, C.-H. Lin, M. Hamada, N. Ohta, and Y.-K. Li, "Time-Gated Imaging on Live Cancer Cells Using Silicon Quantum Dot Nanoparticles with Long-Lived Fluorescence," ACS Photonics **4**, 1306–1315 (2017), publisher: American Chemical Society.

[53] M. Umezawa, K. Miyata, K. Okubo, and K. Soga, en"Three Dimensional Lifetime-Multiplex Tomography Based on Time-Gated Capturing of Near-Infrared Fluorescence Images," Applied Sciences **12**, 7721 (2022), number: 15 Publisher: Multidisciplinary Digital Publishing Institute.

[54] J. W. Walton, A. Bourdolle, S. J. Butler, M. Soulie, M. Delbianco, B. K. McMahon, R. Pal, H. Puschmann, J. M. Zwier, L. Lamarque, O. Maury, C. Andraud, and D. Parker, en"Very bright europium complexes that stain cellular mitochondria," Chemical Communications **49**, 1600–1602 (2013), publisher: The Royal Society of Chemistry.

[55] J. Choi, A. J. Taal, W. L. Meng, E. H. Pollmann, J. W. Stanton, C. Lee, S. Moazeni, L. C. Moreaux, M. L. Roukes, and K. L. Shepard, "Fully Integrated Time-Gated 3D Fluorescence Imager for Deep Neural Imaging," IEEE Transactions on Biomedical Circuits and Systems **14**, 636–645 (2020), conference Name: IEEE Transactions on Biomedical Circuits and Systems.

[56] L. Pancheri, N. Massari, and D. Stoppa, "SPAD Image Sensor With Analog Counting Pixel for Time-Resolved Fluorescence Detection," IEEE Transactions on Electron Devices **60**, 3442–3449 (2013), conference Name: IEEE Transactions on Electron Devices.

[57] F. Guerrieri, S. Tisa, A. Tosi, and F. Zappa, "Two-Dimensional SPAD Imaging Camera for Photon Counting," IEEE Photonics Journal **2**, 759–774 (2010), conference Name: IEEE Photonics Journal.

[58] J. Buchholz, J. W. Krieger, G. Mocsár, B. Kreith, E. Charbon, G. Vámosi, U. Kebschull, and J. Langowski, EN"FPGA implementation of a 32x32 autocorrelator array for analysis of fast image series," Optics Express **20**, 17767–17782 (2012), publisher: Optica Publishing Group.

[59] S. Oasa, A. J. Krmpot, S. N. Nikolić, A. H. A. Clayton, I. F. Tsigelny, J.-P. Changeux, L. Terenius, R. Rigler, and V. Vukojević, "Dynamic Cellular Cartography: Mapping the Local Determinants of Oligodendrocyte Transcription Factor 2 (OLIG2) Function in Live Cells Using Massively Parallel Fluorescence Correlation Spectroscopy Integrated with Fluorescence Lifetime Imaging Microscopy (mpFCS/FLIM)," Analytical Chemistry **93**, 12011–12021 (2021), publisher: American Chemical Society.

[60] M. Vitali, D. Bronzi, A. J. Krmpot, S. N. Nikolić, F.-J. Schmitt, C. Junghans, S. Tisa, T. Friedrich, V. Vukojević, L. Terenius, F. Zappa, and R. Rigler, "A Single-Photon Avalanche Camera for Fluorescence Lifetime Imaging Microscopy and Correlation Spectroscopy," IEEE Journal of Selected Topics in Quantum Electronics **20**, 344–353 (2014), conference Name: IEEE Journal of Selected Topics in Quantum Electronics.

[61] en"Fluoro-Max Fluorescent Streptavidin-Coated Particles," ().

[62] "Europium Chelate For Time-Resolved Fluorescence," (2019).

[63] "High-Speed Photo-Systeme Manual NANOLITE Nanosecond-Flashlamp KL-M," ().

[64] "Coating Curve 357 nm Fluorescence Bandpass Filter: 48 nm FWHM OD>6.0 Coating Performance," (2009).

[65] "Imaging performance specification FLIR Chameleon 3 USB3 Vision Version 4.1," (2017).